Available online at www.sciencedirect.com
SCIENCE DIRECT®
Physics of the Earth and Planetary Interiors 154 (2006) 70–84
PHYSICS OF THE EARTH AND PLANETARY INTERIORS
www.elsevier.com/locate/pepi

Wavelet filter analysis of atmospheric pressure effects in the long-period seismic mode band

X.-G. Hu [a,b,*], L.-T. Liu [a], J. Hinderer [c], H.T. Hsu [a], H.-P. Sun [a]

[a] *Institute of Geodesy and Geophysics, Chinese Academy of Sciences, 340 Xudong Street, Wuhan, China*
[b] *Graduate School of Chinese Academy of Sciences, Beijing, China*
[c] *Institut de Physique du Globe de Strasbourg (UMR 7516 CNRS-ULP), 5 rue Descartes, 67084 Strasbourg Cedex, France*

Received 22 June 2005; received in revised form 19 September 2005; accepted 20 September 2005

Abstract

The importance of the reduction of atmospheric pressure effects becomes very clear when investigating seismic normal-mode spectra below 1.5 mHz. The usual simple correction method consists in subtracting a term converted from local atmospheric pressure (pressure multiplied by a frequency-independent admittance) from the gravity record in time domain. Thus, estimating an efficient admittance is the key for an improved correction. Band-pass filters derived from dyadic orthogonal wavelet transform, having narrow pass-bands with good frequency response but without Gibbs phenomenon and causing no phase lag, are very helpful to estimate an efficient admittance, which is both time and frequency-dependent. Processing of high quality superconducting gravimeter (SG) records for the great Sumatra earthquake (Mw = 9.3, Dec 26, 2004) with wavelet filters reveal the three very well resolved splitting singlets of overtone ${}_2S_1$ with a single gravity record after correction with time-dependent and frequency-dependent admittances. We also observe all coupled toroidal modes below 1.5 mHz, except ${}_0T_5$, ${}_0T_7$ and ${}_1T_1$, with good signal-to-noise ratio (SNR); moreover, toroidal modes ${}_1T_2$ and ${}_1T_3$ are for the first time unambiguously revealed in vertical components.

Keywords: Wavelet filter; Pressure correction; Free oscillations; Superconducting gravimeter

1. Introduction

The Earth can be excited by large earthquakes and starts emitting the seismic energy in oscillatory modes within a frequency range from 0.3 to 20 mHz. These modes can be represented as spheroidal and toroidal modes according to their displacement fields. Toroidal modes only have horizontal displacement component. But the coupling between spheroidal and toroidal modes due to Earth's ellipticity and rotation causes the toroidal modes to appear on the vertical gravimeter records. In the frequency bands below 1.5 mHz, some spheroidal and coupled toroidal modes can rarely be observed with good signal-to-noise ratio (SNR) because of their very weak signals and strong environment and instrumental noise at low frequencies.

The atmospheric noise in gravity signals is due to Newtonian attraction of air mass and vertical displacement of ground caused by atmospheric loading. In study of earth tide gravity variations, it has become a standard method to reduced the pressure effects from the gravity signal by subtracting a pressure converted term, i.e. simultaneously recorded local atmospheric pressure

* Corresponding author. Tel.: +86 27 68881332; fax: +86 27 86783841.
E-mail address: hxg432@sohu.com (X.-G. Hu).

0031-9201/$ – see front matter © 2005 Elsevier B.V. All rights reserved.
doi:10.1016/j.pepi.2005.09.003

multiplied by pressure admittances (e.g. Warburton and Goodkind, 1977; Spratt, 1982; Richter, 1983). Accurate estimation of local atmospheric pressure effects has been studied for long periods (e.g. Doi et al., 1991; Merriam, 1992, 1994; Mukai et al., 1995; Neumeyer, 1995; Neumeyer et al., 1998; Kroner and Jentzsch (1999); Meurers, 1999; Crossley et al., 1995, 2002).

Zürn and Widmer (1995) first showed that pressure correction with a single admittance value around $-3.5\,\mathrm{nm\,s^{-2}\,h\,Pa^{-1}}$ can significantly improve the resolution in observing long-period seismic normal modes at frequencies below 1.5 mHz with the gravity record of a spring instrument. Virtanen (1996), Freybourger et al. (1997) and Van Camp (1999) demonstrated that this method is equally efficient for superconducting gravimeter (SG) record. The simple correction method has now been widely applied for the observation of long-period seismic mode based on the analysis of gravimeter records. In fact the correction method is based on the simple linear model $\Delta p/\Delta g = \alpha$, Thus, estimation of the factors α, the so-called pressure admittance, is the key to efficient pressure correction. The atmospheric effects vary with time, for example, strong pressure effects during the passage of cold fronts (e.g. Müller and Zürn, 1983) and in winter of Europe (e.g. Beauduin et al., 1996), and also vary with frequency (e.g. Warburton and Goodkind, 1977; Merriam, 1994; Neumeyer, 1995; Crossley et al., 1995; Hu et al., 2005). It is reasonable to believe that it is more efficient to correct the pressure effects with time and frequency-dependent admittances.

We propose wavelet method to estimate the time and frequency-dependent admittances. The wavelet bandpass filters based on high-order Daubechies wavelet (Daubechies, 1988) have three advantages over the usual FIR digital filter when processing gravity signals: filtering a signal into narrow frequency bands with good frequency response but causing no phase shift, exhibiting no Gibbs phenomenon and suppressing some singularities. In the following sections, we first introduce the theory of wavelet filter. Then we analyze local atmospheric pressure effects on gravity variations in the long-period seismic mode bands with wavelet method. Finally, we demonstrate that wavelet method and admittances derived from it are very efficient in sharpening up the resolution of the multiplets of ${}_2S_1$, and show the observation of coupled toroidal modes below 1.5 mHz.

2. Bandpass filter derived from wavelet transform

It is well known that a Fourier series uses sins and cosines as orthonormal basis functions to represent a signal. A discrete signal $f_N(t)$ can also be expressed as a wavelet expansion by orthonormal basis derived from two closely related basic functions, scaling function $\phi(t)$ and wavelet $\psi(t)$.

$$f_N(t) = \sum_{n=0}^{N/2^J-1} a_J(n)\, 2^{J/2}\phi(2^J t - n) + \sum_{j=1}^{J}\sum_{n=0}^{N/2^j-1} d_j(n)\, 2^{j/2}\psi(2^j t - n) \quad (1)$$

where J, j and n are integer indices, N is the length of the discrete signal and $N = 2^M$, $0 < J < M$. The above expansion means that by scaling and translating $\phi(t)$ and $\psi(t)$, the scaling function family $2^{J/2}\phi(2^{J/2}t - n)$ and wavelet family $2^{j/2}\psi(2^{j/2}t - n)$ can form an orthonormal basis for the signal. Decomposition coefficients $d_j(n)$ are known as the dyadic discrete wavelet transform of the signal and $a_J(n)$ is a approximation of the signal at scale 2^{-J}. Orthogonal wavelet dilated by 2^j carries signal variations at the resolution 2^{-j}. Thus, Eq. (1) is multi-resolution analysis (MRA) (Mallat, 1989a) of the signal within time scale 2^J. The scaling function $\phi(t)$ and wavelet $\psi(t)$ used to construct the orthonormal basis are derived from two-scale equations (Mallat, 1989a):

$$\phi(t) = \sum_k h(k)\phi(2t - k)$$
$$\psi(t) = \sum_k g(k)\phi(2t - k) \quad (2)$$

where k is an integer index for the infinite or finite sum, $h(k)$, $g(k)$ are sequence called scaling coefficients and wavelets coefficients, respectively. Daubechies (1988, 1992) demonstrated that it is possible for the scaling function and the wavelet to have compact support (i.e. be nonzero only over a finite-region). In such a case, coefficients $g(k)$ and $h(k)$ have a finite even length L, and they are required by orthogonality to be related by

$$g(k) = (-1)^k h(L - 1 - k) \quad k = 0, 1, \ldots, L - 1. \quad (3)$$

Fig. 1 shows Daubechies scaling function and wavelet with length of 128 and discrete-time Fourier transform of them. We can see that scaling function works as low-pass filter and wavelet as high-pass filter. Thus, for the signal in Nyquist frequency band 0–F, within time scale 2^{-J} multi-resolution analysis splits the signal into $J + 1$ logarithmically spaced frequency sub-bands. The first summation in Eq. (1) gives a approximation part of the signal in lower frequency sub-band 0–$F/2^J$. For each index j in the second summation gives J detail

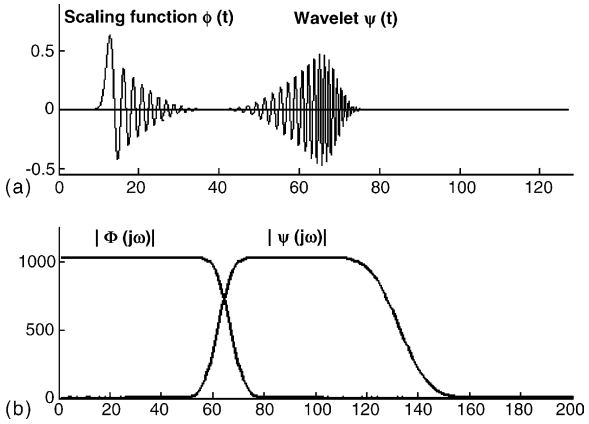

Fig. 1. Daubechies scaling function $\phi(t)$ and wavelet $\psi(t)$ with length of 128 in the time domain (a) and frequency domain (b).

parts in higher frequency sub-band $F/2^j$–$F/2^{j-1}$, $j = 1, 2, \ldots, J$.

Mallat (1989b) proposed a fast algorithm for the multi-resolution analysis of a signal. The algorithm is an iteration procedure which carries out from coefficients to coefficients and orthonormal basis functions never actually enter into the calculation but scaling coefficients $h(k)$ and wavelet coefficients $g(k)$ are used. An analysis procedure determines all decomposition coefficients in Eq. (1) by using two recursion equations:

$$a_{j+1}(n) = 2^{-1/2} \sum_{k=0}^{N/2^j-1} h(k-2n) a_j(k)$$

$$d_{j+1}(n) = 2^{-1/2} \sum_{k=0}^{N/2^j-1} g(k-2n) a_j(k)$$

$$n = 0, 1, 2, \ldots, N/2^{j+1} - 1 \qquad (4)$$

In practice, the discrete signal $f_N(t)$ is usually taken as the initial approximation coefficients $a_0(n)$ ($n = 0, 1, 2, \ldots, N-1$) to the underlying continuous signal at scale index 0.

A synthesis procedure to calculate Eq. (1) from decomposition coefficients $a_j(n)$ and $d_j(n)$ is determined by Eq. (4) as

$$a_{j-1}(k) = 2^{-1/2} \sum_{n=0}^{N/2^j-1} a_j(n) h(k-2n) + 2^{-1/2} \sum_{n=0}^{N/2^j-1} d_j(n) g(k-2n)$$

$$k = 0, 1, 2 \ldots, N/2^{j-1} - 1 \qquad (5)$$

Note that sequence $a_0(k)$ is just the original signal $f_N(t)$.

There is exactly equivalence between Mallat's algorithm and a two-channel orthogonal filter bank (e.g. Smith and Barnwell, 1986). The orthogonal filter bank is a structure that decomposes a signal into a collection of sub-band signals and can perfectly reconstruct the original signal with these sub-band signals. The wavelet two-channel orthogonal filter bank consists of both analysis and synthesis filter bank. The analysis bank is a set of half band low-pass and high-pass filters linked by down-sampling operators (see Fig. 3). The low-pass filter $\bar{h}(k)$ is associated with the scaling function by $\bar{h}(k) = 2^{-1/2} h(L-1-k)$ and high-pass filter $\bar{g}(k)$ is associated with wavelet by $\bar{g}(k) = 2^{-1/2} g(L-1-k)$. The decomposition coefficients $a_J(n)$ and $d_j(n)$ are sub-band signals output by the analysis filter bank in sub-band 0–$F/2^{J+1}$ and $F/2^j$–$F/2^{j-1}$, $j = 1, 2, \ldots, J$. The synthesis filter bank is a set of half band low-pass and high-pass filters linked by up-sampling operators (see Fig. 3). The low-pass filter is $\tilde{h}(k) = 2^{-1/2} h(k)$ and high-pass filter $\tilde{g}(k) = 2^{-1/2} g(k)$. Considering Eq. (3), the half band filters in synthesis bank are associated with these in analysis bank by

$$\begin{aligned} \tilde{h}(k) &= \bar{h}(L-1-k) \\ \tilde{g}(k) &= \bar{g}(L-1-k) \end{aligned} \qquad k = 0, 1, 2, \ldots, L-1 \qquad (6)$$

In such a case, the filter bank is quadrature mirror filter (QMF) bank. The alias, amplitude distortion and phase shift caused by sampling and filtering are cancelled by the special relation between filter $\bar{h}(k)$, $\bar{g}(k)$, $\tilde{h}(k)$ and $\tilde{g}(k)$. Fig. 2 shows the frequency response and phase spectra of these filters. We can see there are mirror symmetry between half-band filters in analysis bank and these in synthesis bank, which leads to no phase shift for the output of wavelet band-pass filter.

The synthesis filter bank can perfectly reconstruct the input signal with the decomposition coefficients from the analysis bank. The orthogonal filter-bank acts as a band-pass filter when only parts of these coefficients are used to reconstruct. The wavelet filtering scheme is shown in Fig. 3. We can see that wavelet analysis bank only repeatedly split, filter and decimate the low-pass bands. This results in logarithmic frequency resolution; the low frequencies have narrow bandwidths and the high frequencies have wide bandwidth. The wavelet packet system proposed by Coifman and Wickerhauser (1992) allows splitting both the low-pass and high-pass bands, and thus leads to a completely evenly spaced frequency band and a finer resolution in high frequency. The multi-resolution of the discrete $f_N(t)$ from wavelet

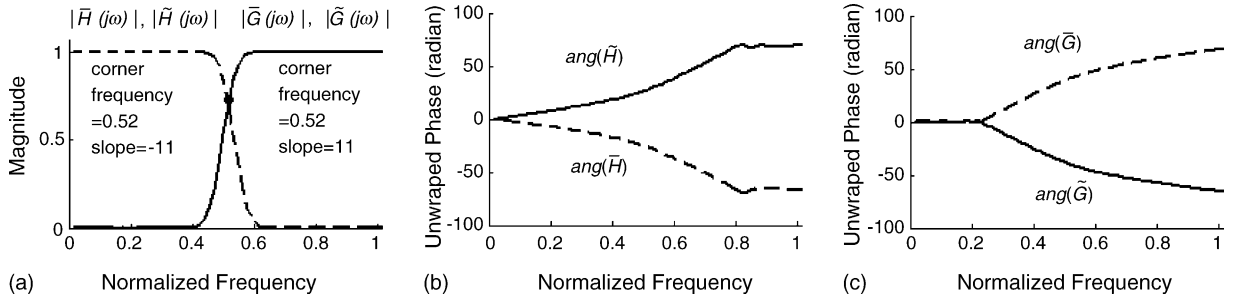

Fig. 2. (a) Frequency response of half-band low-pass and high-pass filters in wavelet QMF bank. (b) Phase spectra of half-band low-pass filter in analysis bank (dashed line) and in synthesis bank (solid line). (c) Phase spectra of half-band high-pass filter in analysis bank (dashed line) and in synthesis bank (solid line).

packet system is expressed as

$$f_N(t) = \sum_{j=1}^{J} \sum_{m=0}^{2^j-1} \sum_{n=0}^{N/2^j-1} w_{j,m}(n)\, 2^{j/2} W_{2^j+m}(2^j t - n) \tag{7}$$

where j is scale index, N the length of the discrete signal and $N = 2^M$, $0 < J < M$. $w_{j,m}(n)$ are wavelet packet decomposition coefficients. The wavelet packet function $W(t)$ is derived from scaling function $\phi(t)$ by recursion equations

$$\begin{aligned} W_{2k}(t) &= \sum_k h(k) W_k(2t-k) \\ W_{2k+1}(t) &= \sum_k g(k) W_k(2t-k) \end{aligned} \tag{8}$$

where $h(k)$, $g(k)$ are scaling and wavelets coefficients, respectively, and $W_0(t)$ is the scaling function $\phi(t)$. The wavelet-packet multi-resolution is implemented with an orthogonal filter bank having a full binary tree structure. For a J-level wavelet-packet filter bank, the discrete signal can be decomposed into 2^J evenly spaced frequency sub-bands: $(n-1)F/2^J$–$nF/2^J$, $n = 1, 2, 3, \ldots, 2^J$. Fig. 4 shows filtering scheme of a three-level wavelet packet filter bank.

The filter bank derived from Daubechies wavelet also has the ability to suppress short-term singularities in the signal. The reason is because of vanishing moment of Daubechies wavelet. The moment condition of Daubechies wavelets can be expressed in terms of the scaling coefficients as

$$\sum_{k=0}^{L-1} (-1)^k h(k) k^m = 0 \quad m = 0, 1, 2, \ldots, L/2 - 1 \tag{9}$$

where L is the length of scaling coefficients $h(k)$. These wavelets have $L/2$ vanishing moments, which means that they can suppress parts of the signal which are polynomial up to degree $L/2-1$. When gravity signals are filtered in to a sub-band, some short-term noise approximated by polynomials of low degree can be suppressed, the harmonic components, such as Earth tides and long-period seismic modes, are smoothly represented. Thus, wavelet filtering is particularly suited to accurately filter out the harmonic components from gravity record.

In the next section we apply the Daubechies wavelet packet filter bank to gravity and local atmospheric pres-

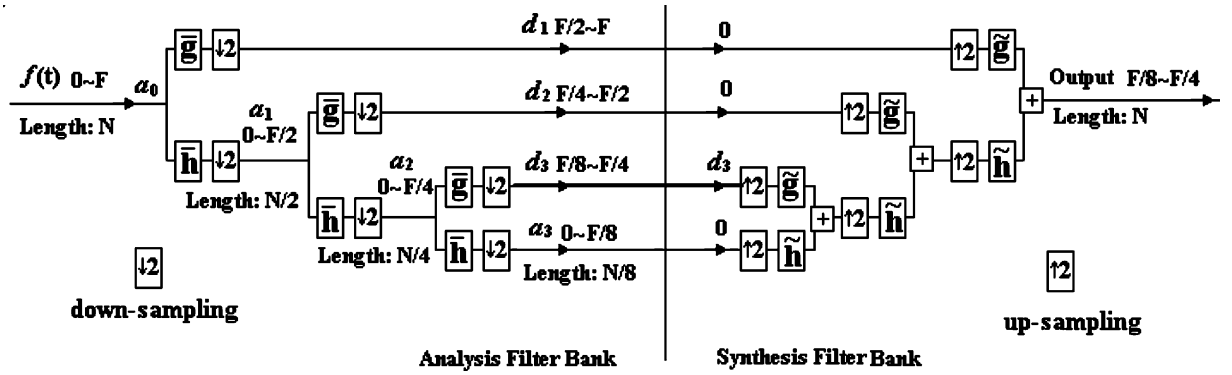

Fig. 3. The three-level wavelet analysis filter bank decomposes an input signal $f(t)$ within Nyquist frequency band 0–F into four sub-band signals a_3, d_1, d_2 and d_3. Synthesis filter banks reconstruct the input signal only with d_3, thus the output, which has the same length as the input signal, is located in sub-band $F/2^3$–$F/2^2$.

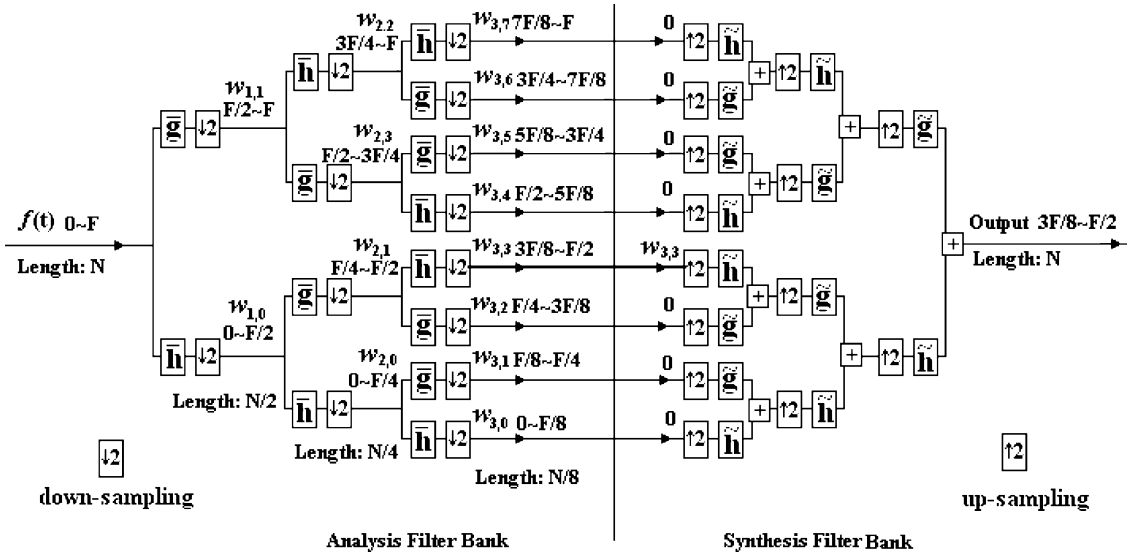

Fig. 4. The three-level wavelet packet analysis filter bank decomposes an input signal $f(t)$ within Nyquist frequency band 0–F into eight sub-band signals. Synthesis filter banks reconstruct the input signal only with $w_{3,3}$, thus the output, which has the same length as the input signal, is in sub-band $3F/2^3$–$4F/2^3$.

sure records to analyze the atmospheric effects in long-period seismic band.

3. Atmospheric pressure effects in long-period seismic band

Until now about 20 superconducting gravimeters (SGs) have been deployed worldwide for measuring temporal gravity variations due to their high sensitivity and low drift rates and their records are collected and exchanged at Global Geodynamics Project (GGP) (e.g., Crossley et al., 1999; Hinderer and Crossley, 2004) data centre located at the International Centre for Earth Tides (ICET) in Brussels. The ability of SGs to measure normal modes had already been studied for many years (e.g. Kamal and Mansinha, 1992; Richter et al., 1995; Freybourger et al., 1997; Banka and Crossley, 1999; Van Camp, 1999), but these early results demonstrated that SGs are noisier than broadband seismometers STS-1 and even spring gravimeters in the long-period seismic normal mode band. But the case is completely different for the new generation compact type SG (e.g. Warburton and Brinton, 1995; Richter and Warburton, 1998), which has a sensitivity close to the 1 nGal (0.01 nm s^{-2}) level in tidal and long-period seismic mode bands. Recent studies of the SG noise level in seismic band, based on new low-noise model (NLNM) (Peterson, 1993), have shown that for frequencies below 1.5 mHz, the new generation SGs are competitive with the best seismometers, and for frequencies below 1 mHz, they can even reach lower noise levels than that of the STS-1 seismometers (e.g. Rosat et al., 2002; Widmer, 2003). Therefore, SGs are particularly suited to observation of the Earth free oscillations below 1.5 mHz. The large 2004 Sumatra earthquake provides us a very good chance for observation of some hard-to-detect spheroidal modes splitting and toroidal modes coupling below 1.5 mHz with SG records.

The SG records for the Sumatra earthquake are provided by GGP data centre. We select eight gravity and local atmospheric records from six GGP stations: C031 (Canberra, Australia), RT038 (Concepcion, Chile), CD-37 (Sutherland, South African), CD029-L and CD029-R (Wettzell, Germany), CD030-L and CD030-R (Bad Homburg, Germany), C026 (Strasbourg, France). These records are decimated to 1 min, thus their Nyquist frequency band is 0–8.33 mHz (periods 2 min to ∞). Using wavelet packet filters derived from Daubechies wavelet with length of 128, we filter out observed gravity and air pressure signals into eight sub-bands: six sub-bands in frequency range 0.26–1.04 mHz with bandwidth 0.13 mHz and two sub-bands in frequency range 1.04–2.08 mHz with bandwidth 0.52 mHz (see Table 1). The admittances between gravity and local atmospheric pressure signals in these sub-bands are determined by a linear regression transfer function as

$$g_c(\Delta t, \Delta f) = g_o(\Delta t, \Delta f) + \alpha(\Delta t, \Delta f)\, p(\Delta t, \Delta f) \quad (10)$$

Table 1
Admittances for eight SG records in eight sub-bands of frequency band 0.26–2.08 mHz, time series is 120 h

Sub-bands (mHz)	0.26–0.39		0.39–0.52		0.52–0.65		0.65–0.78		0.78-0.91		0.91–1.04		1.04–1.56		1.56–2.08	
	α	Corr.	α	Corr.	α	Corr.	α	Corr.	α	Corr.	α	Corr.	α	Corr.	α	Corr.
C026	3.966	0.97	3.470	0.94	3.196	0.93	2.995	0.88	2.651	0.86	2.011	0.74	1.582	0.56	0.032	0.01
CD029_L	3.866	0.92	3.489	0.84	3.343	0.79	2.793	0.73	2.481	0.66	2.149	0.52	1.846	0.42	0.866	0.18
CD029_U	3.864	0.91	3.406	0.82	3.405	0.74	2.891	0.73	2.721	0.70	2.225	0.54	1.921	0.44	0.718	0.17
CD030_L	3.523	0.93	3.101	0.91	3.208	0.88	2.942	0.82	3.169	0.83	2.750	0.78	2.412	0.66	1.944	0.49
CD030_U	3.602	0.89	3.142	0.90	3.230	0.85	2.537	0.80	3.206	0.82	2.650	0.74	2.202	0.60	1.917	0.49
C031	3.451	0.89	3.270	0.76	2.540	0.68	3.14	0.66	1.570	0.48	1.514	0.38	1.359	0.44	0.627	0.14
CD037_L	3.450	0.72	3.394	0.67	2.468	0.50	3.218	0.61	1.907	0.32	2.163	0.41	1.415	0.21	0.471	0.05
RT038	4.074	0.82	3.416	0.70	3.240	0.51	1.981	0.32	2.587	0.30	1.752	0.22	1.675	0.04	2.243	0.13

α is the absolute value of admittance in nm s^{-2} h Pa^{-1} and Corr. is the absolute value of correlation coefficient.

where $g_o(\Delta t, \Delta f)$, $p(\Delta t, \Delta f)$ is the gravity and pressure signals in one of the eight sub-bands Δf set by wavelet packet filters, and $g_c(\Delta t, \Delta f)$ is the corrected gravity. Time interval Δt is selected to be 120 seismically quiet hours before the earthquake because efficient admittances can only be properly estimated when gravity signals are free from other non-atmospheric effects. The admittance $\alpha(\Delta t, \Delta f)$ is calculated by minimizing $|g_c(\Delta t, \Delta f)|^2$ in a least squares sense. The admittance obtained in such a way is both time- and frequency-dependent. The cross-correlations between pressure and gravity in these bands are calculated to judge to which extent pressure fluctuations interfere with gravity variations.

It can be noted immediately from Table 1 that admittances in the long-period normal mode band show significant frequency variability, varying between large values at low frequency and small ones at high frequency. For a comparison, we calculate frequency-domain admittances for the station in Strasburg using the method proposed by Crossley et al. (1995). The linear regression transfer function in the frequency domain as

$$G_c(f) = G_o(f) + \alpha(f)P(f) \tag{11}$$

where $G_o(f)$ and $P(f)$ are the discrete Fourier transform of the tide free gravity residual and pressure signals, and $\alpha(f)$ is the fitting factor. Minimizing $|G_c(f)|^2$ over a narrow frequency bands in a least squares sense leads to

$$\tilde{\alpha}(f) = \frac{\sum \tilde{G}(f)P(f)}{\sum |P(f)|^2} \tag{12}$$

where $\tilde{\alpha}(f)$ is conjugate of factor $\alpha(f)$, which is equivalent to the complex admittance defined by Warburton and Goodkind (1977) from the cross-spectrum of gravity and pressure signals. $\alpha(f)$ can give estimation of admittance and phase difference between the pressure and gravity signals. The admittance estimated in such a way is frequency-dependent but almost time-independent.

The comparison in Table 2 shows that there is only a marginal difference between the admittances from wavelet method and the frequency-domain admittances in high correlation situation. The following reasons can explain the difference: one main reason is due to the application of discrete Fourier transform to gravity and pressure signals. A signal in the frequency domain only has frequency information (i.e. the magnitude of amplitude at a given frequency) but no time information in frequency (when the amplitude occurred). Estimation of admittances in the frequency domain actually assumes that all of the gravity amplitude at a frequency is totally induced by the pressure amplitude at this frequency, but sometimes the pressure is only partly contributing. The hanning taper, which is used to reduce frequency leakage caused by performing Fourier transform for a finite

Table 2
Comparison of admittances between wavelet method solutions and frequency domain solutions

Sub-bands (mHz)	0.26–0.39	0.39–0.52	0.52–0.65	0.65–0.78	0.78–0.91	0.91–1.04	1.04–1.56	1.56–2.08
Wavelet method[a] solutions	3.966	3.470	3.196	2.995	2.651	2.011	1.582	0.032
Frequency domain[a] solutions	3.761	3.313	3.282	2.781	2.483	2.177	1.545	0.538
Phase delay[b] (°)	178.1	179.4	173.8	174.5	172.8	178.9	171.4	91.7
Correlation coefficient	−0.97	−0.94	−0.93	−0.88	−0.86	−0.74	−0.56	−0.01

[a] The absolute value of admittance is in nm s^{-2} h Pa^{-1}.
[b] 180° implies no delay.

length discrete signal, also contributes to the difference. There are small phase differences between pressure fluctuations and gravity variations (see Table 2), but the present wavelet method, which actually determines the admittance in the time domain, takes into no account the phase difference. This is another reason for the difference. But in trying to precisely reduce the pressure effects from gravity records in the search for the weak geodynamic signals from the Earth's interior, we believe it is appropriate to use the wavelet method advocated in the present paper. This method can take into account both time and frequency information of atmospheric pressure effects. This is the advantage over frequency-domain correction method, which loses most of the time information.

The results from eight SG records in Table 1 show gravity variations highly correlate with atmospheric pressure fluctuations in frequency range 0.26–0.52 mHz. There is very low correlation between the pressure and gravity above 1.5 mHz, because such high frequency components are very weak in the atmospheric pressure signals. Hence, gravity variations at frequencies above 1.5 mHz have other physical origins, and the gravity records in these bands can be contaminated by the pressure correction estimated with a constant admittance. Fig. 5 shows that in Strasbourg SG station the 120-h atmospheric pressure fluctuations fit gravity variations very well in time domain as well as in frequency domain in frequency band 0.26–0.39 mHz using the admittance $\alpha(120,\ 0.26\text{–}0.39) = -3.966\,\mathrm{nm\,s^{-2}\,h\,Pa^{-1}}$ calculated by Eq. (2).

In long-period normal mode band, admittances sometimes conspicuously change on time scales of hours to days with the variations of local atmospheric pressure. To show such a case, we consider pressure effects at Strasbourg SG station by selecting two continuous and seismically quiet days, the first day with appreciable and the second with small variations in atmospheric pressure. Fig. 6 shows that in frequency band 0.26–0.39 mHz strong atmospheric pressure fluctuations lead to a large admittance absolute value of $4.150\,\mathrm{nm\,s^{-2}\,h\,Pa^{-1}}$ and a high correlation coefficient of -0.987 for the first day, but admittance and correlation coefficients become $3.006\,\mathrm{nm\,s^{-2}\,h\,Pa^{-1}}$ and -0.974, respectively, during the second day because of weaker pressure fluctuations. The standard deviation of gravity signal on the first day is reduced from 0.202 to $0.033\,\mathrm{nm\,s^{-2}}$ and on the second day from 0.163 to $0.037\,\mathrm{nm\,s^{-2}}$ after pressure correction using the time-dependent admittance, demonstrating hence the effectiveness of the wavelet method.

Analysis of gravity and pressure records from other SG station also verifies that admittances in the long-period normal mode band show significantly time variability, with large admittance value and high correlation in the time period of strong air pressure fluctuations. Zürn and Widmer (1995) found that, in long-period seismic

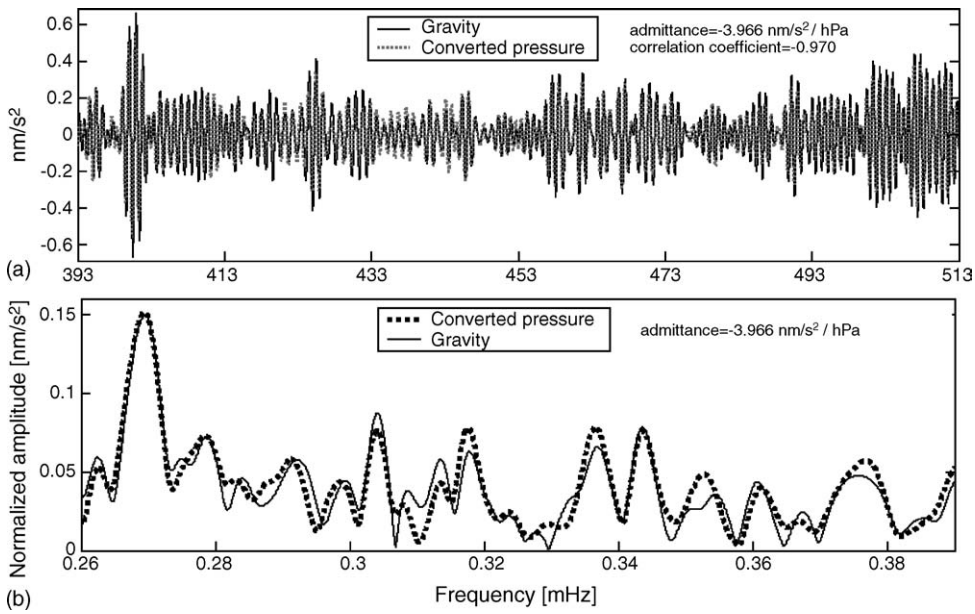

Fig. 5. (a) The time domain local atmospheric pressure signal fits gravity signal well at Strasbourg SG station in frequency range 0.26–0.39 mHz. The solid curve stands for gravity variations and the dot curve for converted pressure, i.e. pressure multiplied by admittance value of $-3.966\,\mathrm{nm\,s^{-2}\,h\,Pa^{-1}}$. The time series is 120 seismically quiet hours before the 2004 Sumatra event. (b) The pressure also fits gravity well in frequency domain. A Hanning taper is applied to the time series before computing discrete Fourier transform.

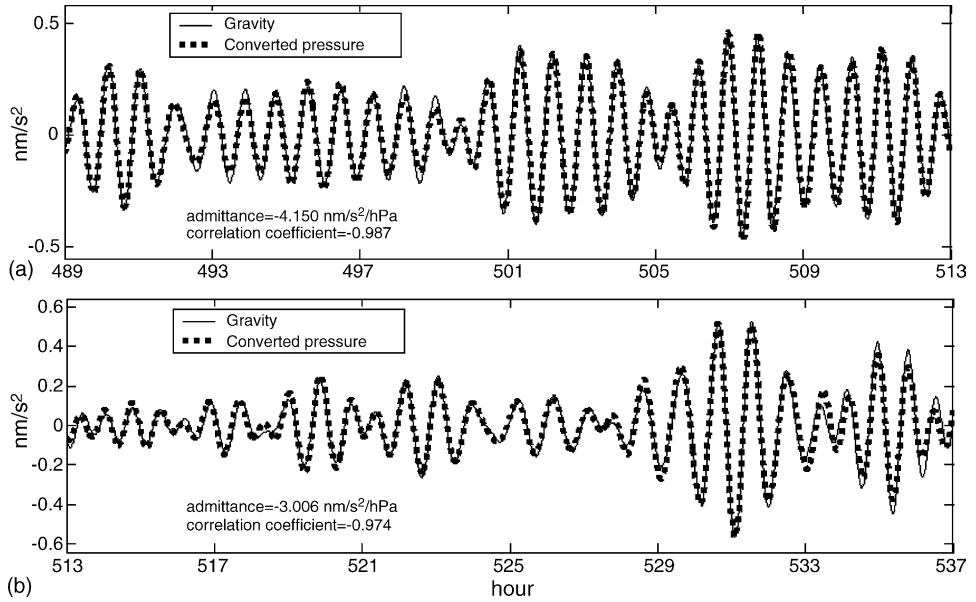

Fig. 6. Two continuous day time series of gravity and local atmospheric pressure at Strasbourg SG station in frequency band 0.26–0.39. (a) Strong local atmospheric pressure fluctuations lead to a large admittance value of $-4.150\,\mathrm{nm\,s^{-2}\,h\,Pa^{-1}}$ for the first day. (b) There is a smaller admittance value of $-3.006\,\mathrm{nm\,s^{-2}\,h\,Pa^{-1}}$ for the second day because of the comparatively weak pressure fluctuations.

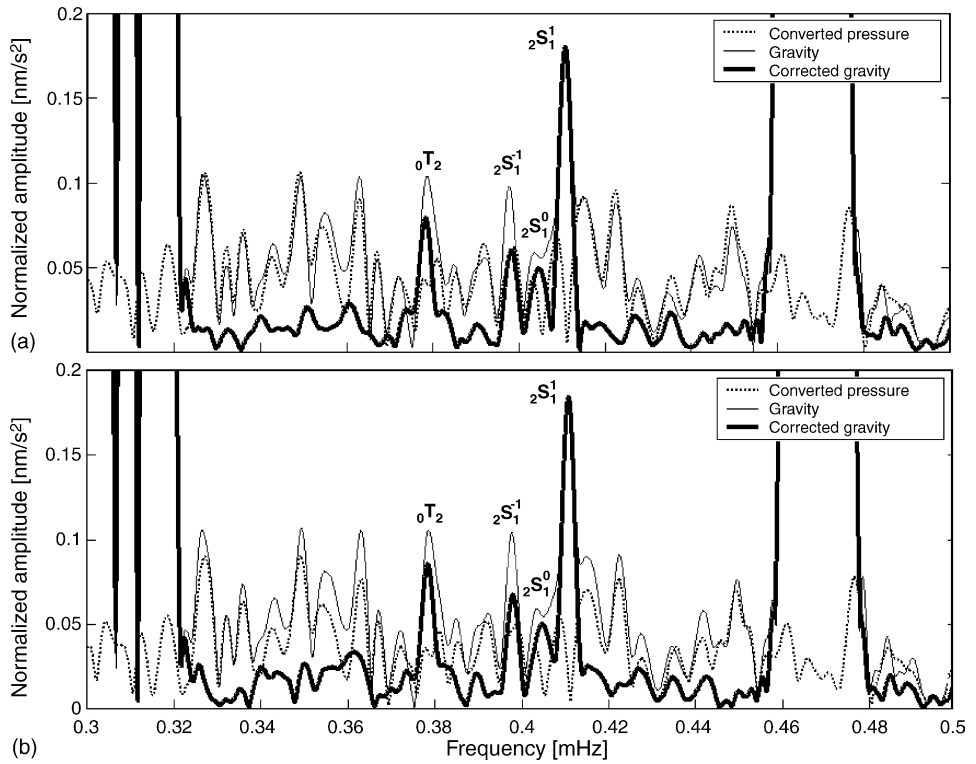

Fig. 7. Linear amplitude spectra around $_2S_l$ for SG C026 (Strasbourg) after the Sumatra event of 26 December 2004. The time window is 5–173 h. A Hanning taper is applied to the time series before computing discrete Fourier transform. (a) Spectrum obtained from the wavelet method with time and frequency-admittance and (b) from the usual method with admittance of $-3\,\mathrm{nm\,s^{-2}\,h\,Pa^{-1}}$. The pressure (dot curve) fits raw gravity (thin curve) better by using the wavelet method than by the usual method and the spectrum of pressure corrected gravity (bold curve) from the wavelet method show higher SNR.

band by using a constant admittance, the noise level in the corrected record in the case of strong atmospheric pressure variations drops to a value lower than that for weaker pressure variations, but they could not give a clear explanation. We believe the dependence of the time-variable admittance with atmospheric pressure variations can explain this fact.

High correlation in sub-band 0.26–1.04 mHz means local atmospheric pressure fluctuations is the major noise origin. The admittance value shows time- and frequency-dependent. When doing atmospheric correction at frequencies below 1 mHz, most of atmospheric noise can be reduced from gravity signals by using the nominal admittance $-3\,\mathrm{nm\,s^{-2}\,h\,Pa^{-1}}$. But when searching for the weak signals, which are almost hidden by the atmospheric noise in seismic band at frequencies below 1 mHz, we believe it is appropriate to use wavelet method and time- and frequency-dependent admittances to reduce pressure effects precisely from gravity records. The observation of the splitting of ${}_2S_1$ is a good example.

4. Observation of splitting of ${}_2S_1$

${}_2S_1$ is the second gravest mode and is the first overtone of ${}_1S_1$, the commonly called Slichter mode (Slichter, 1961), which corresponds to a translation of the inner

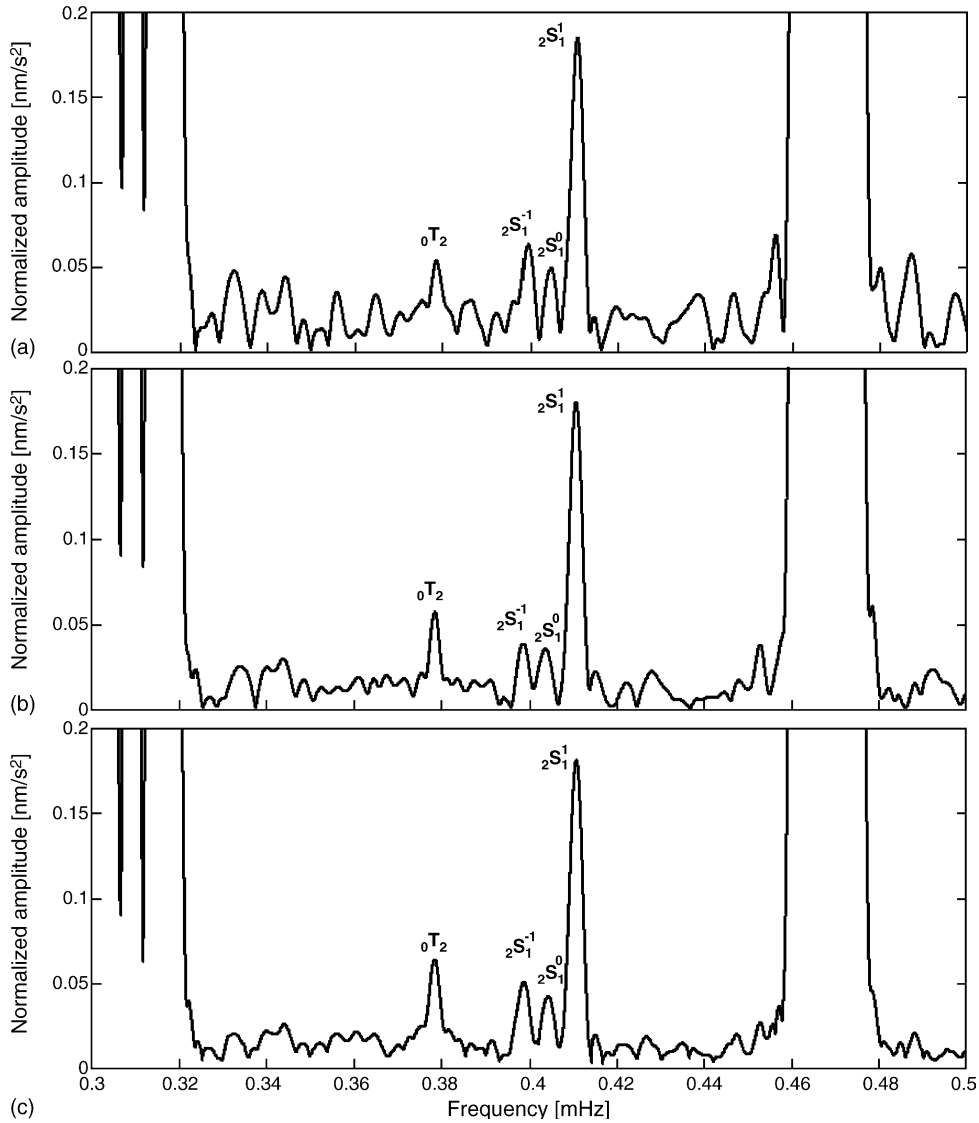

Fig. 8. Linear amplitude spectra around ${}_2S_l$ for (a) SG C029-L (Wettzell) and (b) SG C030-U (Bad Homburg) after the Sumatra event of 26 December 2004. (c) The product spectrum of corrected gravity records from SG station Bad Homburg, Strasbourg and Wettzell. The time window is 5–173 h. A Hanning taper is applied to the time series before computing discrete Fourier transform.

core relative to the mantle. ${}_2S_1$ is such a weak signal that has not been observed until Rosat et al. (2003) revealed it using the multi-station experiment to stack records from five SG stations after the 2001 Peru event with magnitude 8.4. The magnitude 9.3 Sumatra event excited a plethora of free oscillations at frequencies below 1 mHz and, because of the extremely large magnitude, we will show that it is possible to observe the splitting of ${}_2S_1$ with a single SG record.

Fig. 7 shows Fourier spectra of 168-h gravity records from SG C026 for detecting the three multiplet of ${}_2S_1$ by using two different methods. One is the usual method which removes the tides by subtracting synthetic local tides and corrects the local atmospheric pressure effects using a nominal constant admittance of $-3\,\mathrm{nm\,s^{-2}\,h\,Pa^{-1}}$. Another method is the wavelet method which filter signal into sub-band 0.26–0.52 mHz and make pressure correction using two admittance values according to the frequency band; $\alpha(0.26\text{–}0.39) = -3.9$ and $\alpha(0.39\text{–}0.52) = -3.8\,\mathrm{nm\,s^{-2}\,h\,Pa^{-1}}$. Comparing solutions of two methods in Fig. 7, it can be clearly see that the wavelet method is able to extract ${}_2S_1^0$ from atmospheric noise with better resolution. This is the first time the three very well resolved splitting singlets of overtone ${}_2S_1$ have been observed with a single gravity record. A recent similar work by Rosat et al. (2005) shows that the usual method with admittance of $-3\,\mathrm{nm\,s^{-2}\,h\,Pa^{-1}}$

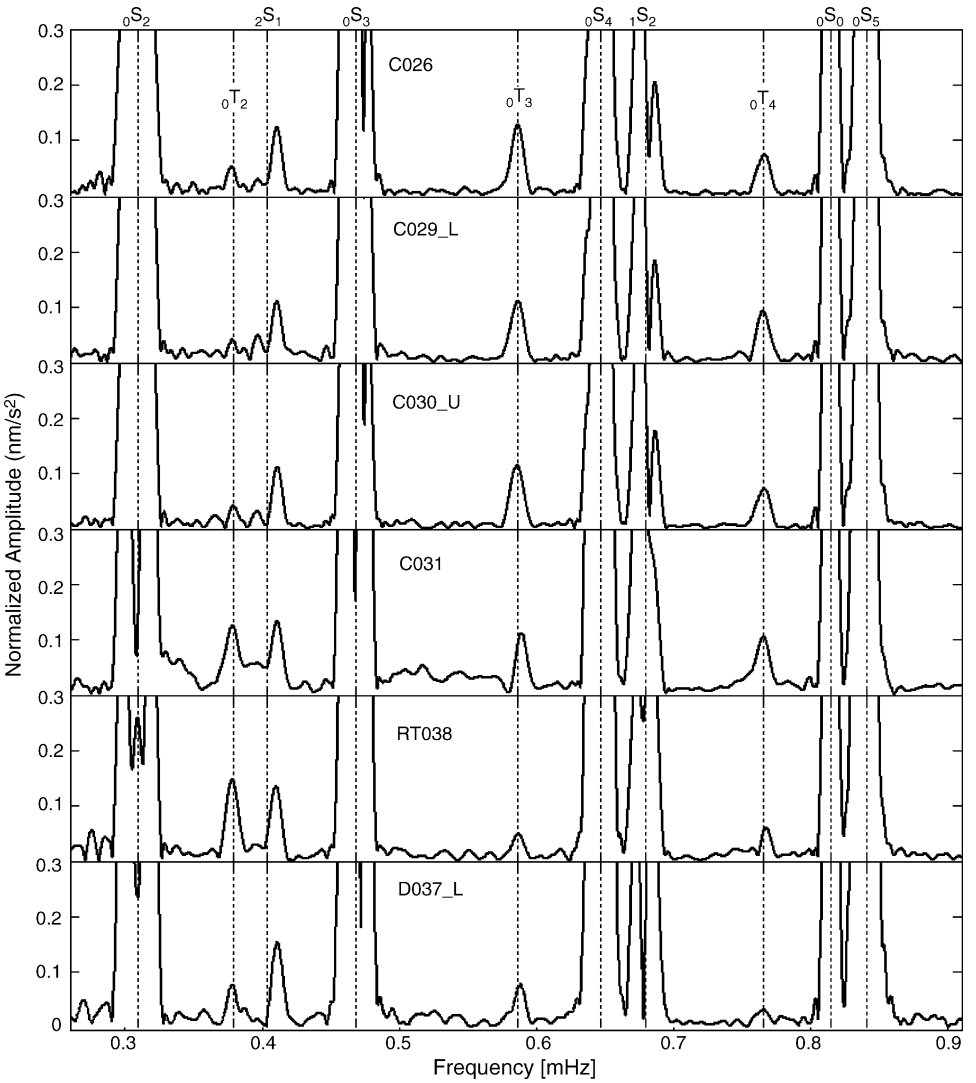

Fig. 9. Amplitude spectra of Hanning-tapered records for modes below 1 mHz for six SGs after the Sumatra event of 26 December 2004. The spectral peaks of the spheroidal modes, which are about 10 times larger than those of the coupled toroidal modes, have been clipped for better display. The time window is 5–65 h; vertical dashed lines indicate the theoretical positions of modes (Masters and Widmer, 1995).

Table 3
Observed frequencies of 2S1 for three methods and predicted values for the Earth Model 1066A

	The wavelet method results (μHz)	The usual method results (μHz)	Product spectrum results (μHz)	Model 1066A[a] result (μHz)
${}_2S_1^{-1}$	398.310 ± 0.051	398.047 ± 0.052	398.854 ± 0.048	398.708
${}_2S_1^{0}$	404.605 ± 0.077	404.770 ± 0.078	404.331 ± 0.075	404.690
${}_2S_1^{1}$	410.835 ± 0.041	410.838 ± 0.042	410.835 ± 0.041	410.880

[a] The split eigenfrequencies of ${}_2S_l$ for 1066A Earth model (Gilbert and Dziewonski, 1975) are determined by using a perturbation method (Dahlen and Sailor, 1979) to the first order in ellipticity and to the second order in rotation.

does not lead to observation of all of three multiplet of ${}_2S_l$ on individual SG spectra. This further confirms that wavelet method can really achieve additional gains in the observation of weak normal modes.

We estimate the observed singlet frequencies derived from the two methods by fitting a synthetic resonance function (Masters and Gilbert, 1983) to each singlet of both spectra. The results are compared in Table 3, in which predicted frequencies of ${}_2S_1$ computed for the earth model 1066A (Gilbert and Dziewonski, 1975) are also included. We can see that the two different pressure corrections lead to differences in the frequency of ${}_2S_1^0$ and ${}_2S_1^{-1}$ observations, and that the observations from the wavelet method are closer to the predicted values, despite that the observed frequency of ${}_2S_1^{-1}$ is still quite smaller than the predicted value. Two gravity records from SG CD029_L (Wettzell) and CD030_U (Bad Homburg) also reveal the three well resolved multiplet peaks of ${}_2S_1$ after pressure correction using wavelet method and admittances in Table 1 (see Fig. 8a and b). Because of the non-negligible impact of atmospheric pressure corrections on the frequency estimates of the singlet ${}_2S_1^0$ and

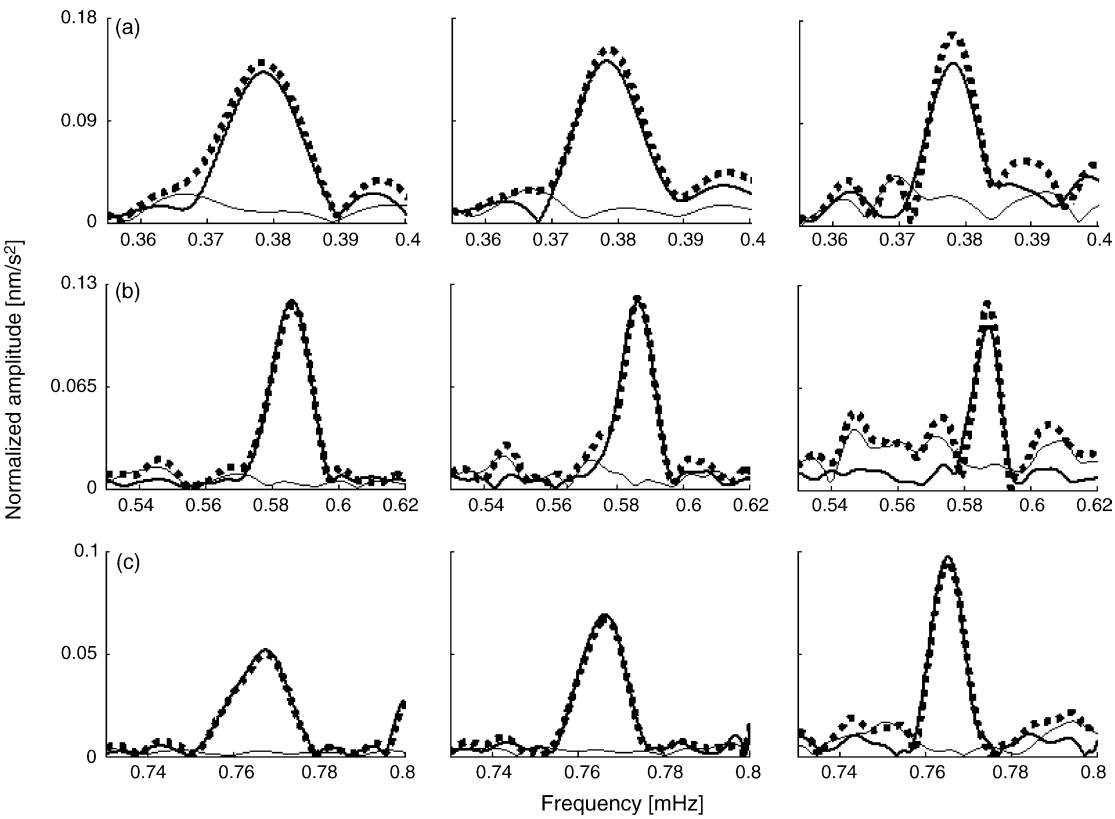

Fig. 10. (a) Time evolution of ${}_0T_2$ recorded by SG RT038 and (b) ${}_0T_3$, (c) ${}_0T_4$ recorded by C026 after the Sumatra event of 26 December 2004. From left to right, the time window is 5–45, 5–55 and 5–75 h, respectively. A Hanning taper is applied to the time series before computing discrete Fourier transform. The bold curve indicates pressure corrected gravity and dot curve is raw gravity. The thin curve is converted pressure.

${}_2S_1^{-1}$, the product spectrum of the three records may produce more reasonable results. The product spectrum is a simple stacking method since it is the geometric mean of the product of the individual spectrum. In the high SNR situation, the product spectrum would show only signals common to all stations, those not present in one or more records being eliminated, and systematic errors affecting individual stations would also be suppressed (Courtier et al., 2000). We can see from Fig. 8c that the product spectrum further sharpens up the resolution of the multiplet of ${}_2S_1$. The frequencies estimated from the product spectrum are also displayed in Table 3.

5. Observation of coupled toroidal modes

The coupling between spheroidal and toroidal modes causes toroidal modes to appear on the vertical gravimeter records. The Coriolis coupling effects at frequencies below 1.5 mHz generate such weak signals that it can rarely be observed with reasonable SNR. Several of coupled toroidal mode, ${}_0T_5$ and ${}_1T_1$ for example are completely overlapped by nearby mulitiplet of spheroidal modes and are irresolvable, and the coupled mode ${}_0T_7$ and ${}_0T_8$ with very low Q attenuate rapidly thus can hardly be observed.

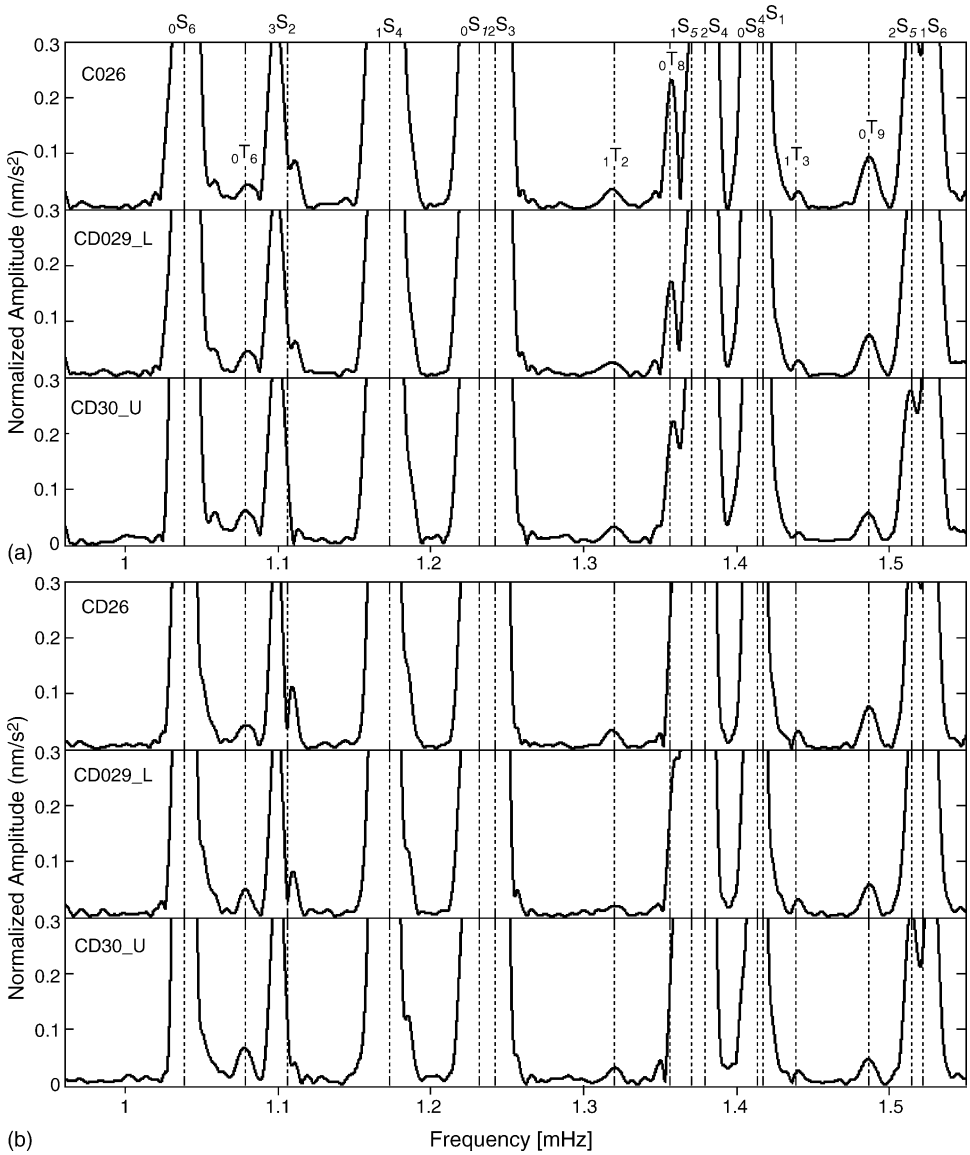

Fig. 11. Amplitude spectra of Hanning-tapered records for modes in frequency band 1–1.5 mHz for SG C026, CD029-L and CD030-U after the Sumatra event of 26 December 2004. (a) The time window is 2–45 h; (b) the time window is 2–62 h. The vertical dashed lines indicate the theoretical positions of the modes (Masters and Widmer, 1995).

Only a strong earthquake with a source mechanism generating large strike-slip fault motion can excite toroidal coupling effects at frequencies below 1 mHz to observable amplitudes for the quietest gravimeters. The recent work by Park et al. (2005) demonstrates that the 26 December 2004 Sumatra Earthquake source actually consists of three large fault rupture events, and one of them is such a large strike-slip event that it is equivalent to a seismic event with Mw = 8.9, by itself larger than any earthquake between 1964 Alaska and 2004 Sumatra. Thus, the large 2004 Sumatra earthquake provides an opportunity for SGs to show these very weak coupling effects.

After pressure correction, the amplitude spectra of 60-h Hanning-tapered SG records for six SG stations show very clear peaks near the theoretical position of ${}_0T_2$, ${}_0T_3$, ${}_0T_4$ (see Fig. 9). To check the influence of the air pressure correction, we compare spectra of raw gravity, corrected gravity and converted pressure around ${}_0T_2$, ${}_0T_3$, ${}_0T_4$. Fig. 10 shows the amplitude evolution of coupled toroidal modes ${}_0T_2$ (recorded by RT038) and ${}_0T_2$, ${}_0T_3$ (recorded by SG C026) with time. It can be noted that local atmospheric pressure fluctuations make very small interference for observing frequencies of coupled modes. Hence, the frequency of these coupled modes can be accurately estimated.

Zürn et al. (2000) reported the first observation of the coupled toroidal modes ${}_0T_2$, ${}_0T_3$ and ${}_0T_4$ at frequencies 374.7 ± 1.5, 586.5 ± 2.0 and 765.0 ± 1.5 μHz, respectively, using data from spring gravimeters and SGs (one is from SG C026 in Strasbourg) after the strike-slip Mw = 8.2 1998 Balleny Island earthquake and correcting the local pressure effects with a constant admittance of $-3.75\,\mathrm{nm\,s^{-2}\,h\,Pa^{-1}}$. The large 2004 Sumatra–Andaman earthquake allows us to identify these coupled modes with much higher SNR. Fitting synthetic resonance function (Masters and Gilbert, 1983) to the observed spectra, we estimate the frequencies of coupled ${}_0T_2$, ${}_0T_3$ and ${}_0T_4$ and obtain 378.23 ± 0.65, 586.34 ± 0.47 and 765.86 ± 0.45 μHz, respectively. Notice that our observations are close to that of Zürn except for the frequency of coupled ${}_0T_2$. After carefully analysis of the SG C026 records for Balleny Island seismic event, we find that local atmospheric pressure highly interferes with the observation of the frequency of coupled ${}_0T_2$, so the removal of pressure effects may explain the difference.

In order to observe the weak and rapidly attenuated coupling mode in the frequency range 1–1.5 mHz, we performed a spectral analysis for gravity records using a short time window 2–47 h. Close inspection of the linear amplitude spectra of the records from the three European SG stations, Strasbourg, Wenzell and Bad Homburg reveals small but clear peaks at the frequencies of coupled ${}_0T_6$, ${}_0T_8$ and ${}_0T_9$; moreover coupled ${}_1T_2$ and ${}_1T_3$ is clearly visible (see Fig. 11a).

These modes have been observed and measured in horizontal components of seismometers (e.g. Tromp and Zanzerkia, 1995; Resovsky and Ritzwoller, 1998) but, to the best of our knowledge there has been no claim for detection of coupled ${}_1T_2$, ${}_1T_3$ from gravimeter records and vertical components of seismometers until now. To further confirm our observation of coupled ${}_1T_2$, ${}_1T_3$, we extended the time window to 2–62 h. Fig. 11b shows ${}_0T_8$ decay away for its very low Q but ${}_1T_2$ and ${}_1T_3$ still are clearly visible.

6. Conclusion

We used a wavelet method to clearly show that the local atmospheric pressure fluctuations highly correlate with gravity at frequencies below 1 mHz in the long-period seismic band, and pressure admittance is not a nominal constant value but varying in a range from 2 to $4\,\mathrm{nm\,s^{-2}\,h\,Pa^{-1}}$, large values at low frequencies and at the time when there are strong pressure fluctuations. Wavelet filters can be very helpful to estimate the admittances which are time-dependent as well as frequency-dependent. The detection of the three very well resolved splitting singlets of mode ${}_2S_1$ using a single SG records fully shows the efficiency of pressure correction with wavelet method. The first observation of coupled mode ${}_1T_2$ and ${}_1T_3$ demonstrates that new generation SGs are also very sensitive for observation of seismic normal mode in frequency band 1–1.5 mHz. We conclude that the use of SG records corrected with wavelet band-pass filters for pressure effects can contribute to the improvement of the SNR of weak signals in the study of long period normal mode seismology.

Acknowledgements

We are grateful to the GGP managers for providing the SG datasets of the Sumatra event. This research is financed by the National Natural Sciences Foundation of China (grant 40574009) and Chinese Academy of Science (CAS) Hundred Talent Program and Innovation Project (No. KZCX3-SW-131) for supporting this research.

References

Banka, D., Crossley, D., 1999. Noise levels of superconducting gravimeters at seismic frequencies. Geophys. J. Int. 139, 87–97.

Beauduin, R., Lognonné, P., Montagner, J.P., Cacho, S., Karczewski, J.F., Morand, M., 1996. Atmospheric pressure changes on seismic signals or how to improve the quality of a station. Bull. Seism. Soc. Am. 86, 1760–1769.

Coifman, R.R., Wickerhauser, M.V., 1992. Entropy-based algorithms for best basis selection. IEEE Trans. Inform. Theory 38 (2), 713–718.

Courtier, N., Ducarme, B., Goodkind, J., Hinderer, J., Imanishi, Y., Seama, N., Sun, H., Merriam, J., Bengert, B., Smylie, D., 2000. Global superconducting gravimeter observations and the search for the translational modes of the inner core. Phys. Earth Planet Int. 117, 3–20.

Crossley, D., Hinderer, J., Casula, G., Francis, O., Hsu, H.-T., Imanishi, Y., Jentzsch, G., Kaarianen, J., Merriam, J., Meurers, B., Neumeyer, J., Richter, B., Shibuya, K., Sato, T., van Dam, T., 1999. Network of superconducting gravimeters benefits a number of disciplines, EOS, 80, 11, 121–126.

Crossley, D., Jensen, O., Hinderer, J., 1995. Effective barometric admittance and gravity residuals. Phys. Earth Planet Int. 90, 221–241.

Crossley, D., Hinderer, J., Rosat, S., 2002. Using the atmosphere-gravity correlation to derive a time-dependent admittance. Bull. Inf. Mar. Terr. 136, 10809–10820.

Daubechies, I., 1988. Orthonormal bases of compactly supported wavelet. Commun. Pure Appl. Math. 41, 909–996.

Daubechies, I., 1992. Ten Lectures on Wavelets, Number 61 in CBMS-NSF Series in Applied Mathematics. SIAM, Philadelphia.

Dahlen, F.A., Sailor, R.V., 1979. Rotational and elliptical splitting of the free oscillations of the Earth. Geophys. J. R. Astron. Soc. 58, 609–623.

Doi, K., Higashi, T., Nakegawa, I., 1991. An effect of atmospheric changes on the time change of gravity observed by a superconducting gravity meter. J. Geod. Soc. Jpn. 37, 1–12.

Freybourger, M., Hinderer, J., Trampert, J., 1997. Comparative study of superconducting gravimeters and broadband seismometers STS-1/Z in subseismic frequency bands. Phys. Earth Planet Int. 101, 203–217.

Gilbert, F., Dziewonski, A., 1975. An application of normal mode theory to the retrieval of structural parameters and source mechanisms from seismic spectra. Philos. Trans. R. Soc. Lond. Ser. A 278, 187–269.

Hinderer, J., Crossley, D., 2004. Scientific achievements from the first period (1997–2003) of the Global Geodynamics Project using a worldwide network of superconducting gravimeters. J. Geodyn. 38, 237–262.

Hu, X.-G., Liu, L.T., Hinderer, J., Sun, H.P., 2005. Wavelet filter analysis of local atmospheric pressure effects on gravity variations. J. Geod., 79, doi:10.1007/s00190-005-0486-6.

Kamal, Mansinha, L., 1992. A test of the superconducting gravimeter as a long-period seismometer. Phys. Earth Planet Int. 71, 52–60.

Kroner, C., Jentzsch, G., 1999. Comparison of different barometric pressure reductions for gravity data and resulting consequences. Phys. Earth. Planet Int. 115, 205–218.

Mallat, S., 1989a. Multiresolution approximations and wavelet orthonormal bases of $L^2(R)$. Trans. Am. Math. Soc. 315, 69–87.

Mallat, S., 1989b. A theory for multiscale signals decomposition: The wavelet representation. IEEE Trans. Pattern Anal. Mach. Intell. 11, 674–693.

Masters, G., Gilbert, F., 1983. Attenuation in the earth at low frequencies. Philos. Trans. R. Soc. Lond. A308, 479–522.

Masters, G., Widmer, R., 1995. Free oscillation: Frequencies, global earth physics, A Handbook of Physical Constants, AGU Reference Shelf Online 1, http://www.agu.org/reference/gephys/9_masters.pdf.

Merriam, J., 1992. Atmospheric pressure and gravity. Geophys. J. Int. 109, 488–500.

Merriam, J., 1994. The nearly diurnal free wobble resonance in gravity measured at Cantley. Qubec Geophys. J. Int. 119, 369–380.

Meurers, B., 1999. Gravitational effects of atmospheric processes in SG gravity data. Cahier du Centre Europeen de Geodynamique et de Seismologie 17, 57–65.

Mukai, A., Higashi, T., Takemoto, S., Nakagawa, I., Naito, I., 1995. Accurate estimation of atmospheric effects on gravity observations made with a superconducting gravity meter at Kyoto. Phys. Earth Planet Int. 91, 149–159.

Müller, T., Zürn, W., 1983. Observations of gravity changes during the passage of cold fronts. J. Geophys. 53 (3), 155–162.

Neumeyer, J., 1995. Frequency-dependent atmospheric pressure correction on gravity variations by means of cross spectral analysis. Bull. Inf. Mar. Terr. 122, 9212–9220.

Neumeyer, J., Barthelmes, F., Wolf, D., 1998. Atmospheric pressure correction for gravity data using different methods. In: Ducarme, B., Paquet, P. (Eds.), Proc. 13th Int. Symp. Earth Tides. July 1997, Brussels, pp. 431–438.

Peterson, J., 1993. Observation and modeling of seismic background noise, U.S. Geol. Surv., Open-File Re 1–45, 93–322.

Park, J., Song, T.R., Tromp, J., Okal, E., Stein, S., Roult, G., Clevede, E., Laske, G., Kanamori, H., Davis, P., Berger, J., Braitenberg, C., Van Camp, M., Lei, X., Sun, H., Xu, H., Rosat, S., 2005. Earth's free oscillations excited by the 26 December 2004 Sumatra–Andaman earthquake. Science 308, 1139–1144.

Richter, B., 1983. Three years of registration with the superconducting gravimeter. Bull. Inf. Mar. Terr. 93, 1–9.

Richter, B., Wenzel, H.G., Zürn, W., Klopping, F., 1995. From Chandler wobble to free oscillations: comparison of cryogenic gravimeters and other instruments in a wide period range. Phys. Earth Planet Int. 91, 131–148.

Richter, B., Warburton, R., 1998. A new generation of superconducting gravimeters enables the in-situ detection and elimination of offsets and interruptions from continuous gravity measurements. In: Ducarme, B. (Ed.), Proc. 13th Int. Symp. Earth Tides. Brussels, pp. 545–555.

Rosat, S., Hinderer, J., Crossley, D., 2002. A comparison of the seismic noise levels at various GGP stations. Bull. Inf. Mar. Terr. 135, 10689–10700.

Rosat, S., Hinderer, J., Rivera, L., 2003. First observation of 2S1 and study of the splitting of the football mode 0S2 after the June 2001 Peru earthquake of magnitude 8.4. Geophys. Res. Lett. 30 (21), 2111, doi:10.1029/2003GL018304.

Rosat, S., Sato, T., Imanishi, Y., Hinderer, J., Tamura, Y., McQueen, H., Qhashi, M., 2005. High-resolution analysis of the gravest seismic normal modes after the 2004 Mw = 9 Sumatra earthquake using superconducting gravimeter data. Geophys. Res. Lett. 32, L13304, doi:10.1029/2005GL018304.

Resovsky, J., Ritzwoller, M., 1998. New and refined constraints on three-dimensional Earth structure from normal modes below 3 mHz. J. Geophys. Res. 103 (1), 783–810.

Slichter, L.B., 1961. The fundamental free mode of the Earth's inner core. Proc. Natl. Acad. Sci. 47, 186–190.

Smith, M., Barnwell, T., 1986. Exact reconstruction for tree-structured subband coders. IEEE Trans. ASSP 34, 431–441.

Spratt, R.S., 1982. Modeling the effect of atmospheric pressure variations on gravity. Geophys. J. R. Astron. Soc. 71, 173–186.

Tromp, J., Zanzerkia, E., 1995. Toroidal splitting observations from the great 1994 Bolivia and Kuril Islands earthquakes. Geophys. Res. Lett. 22, 2297–2300.

Virtanen, H., 1996. Observation of free oscillation of the earth by superconducting gravimeter GWR T-020. Acta Geod. Geophys. Hung. 31, 423–431.

Van Camp, M., 1999. Measuring seismic normal modes with the GWR C021 superconducting gravimeter. Phys. Earth Planet Int. 116, 81–92.

Warburton, R.J., Goodkind, J.M., 1977. The influence of atmospheric pressure variations on gravity. Geophys. J. R. Astron. Soc. 48, 281–292.

Warburton, R.J., Brinton, E.W., 1995. Recent Developments in GWR Instrument's superconducting Gravimeters, in workshop proceedings, Non-tidal gravity changes, Proc. of Second Workshop: Non-tidal gravity changes. Cahiers du Centre Européen de Géodynamique et de Séismologie 11, 23–56.

Widmer, R., 2003. What can superconducting gravimeters contribute to normal mode seismology? Bull. Seism. Soc. Am. 93, 1370–1380.

Zürn, W., Widmer, R., 1995. On noise reduction in vertical seismic records below 2 mHz using local barometric pressure. Geophys. Res. Lett. 22, 3537–3540.

Zürn, W., Laske, G., Widmer, R., Gilbert, F., 2000. Observation of Coriolis coupled modes below 1 mHz. Geophys. J. Int. 143, 113–118.